

Understanding the connection between the energy released during solar flares and their emission in the lower atmosphere

F. Rubio da Costa

Department of Physics, Stanford University, Stanford, CA 94305, USA
email: frubio@stanford.edu

Abstract. While progress has been made on understanding how energy is released and deposited along the solar atmosphere during explosive events such as solar flares, the chromospheric and coronal heating through the sudden release of magnetic energy remain an open problem in solar physics. Recent hydrodynamic models allow to investigate the energy deposition along a flare loop and to study the response of the chromosphere. These results have been improved with the consideration of transport and acceleration of particles along the loop. *RHESSI* and *Fermi*/GBM X-ray and gamma-ray observations help to constrain the spectral properties of the injected electrons. The excellent spatial, spectral and temporal resolution of *IRIS* will also help us to constrain properties of explosive events, such as the continuum emission during flares or their emission in the chromosphere.

Keywords. Sun: flares; chromosphere — hydrodynamics — radiative transfer — line: formation.

1. Introduction

Solar flares involve many processes and multiple chains of events. These can be grouped in three major parts: the energy build up and release through reconnection, the particle acceleration-transport and energizing of coronal plasma, and the response of the lower atmosphere to this energy input. Here, we will focus on the last two points.

The chromosphere is particularly difficult to model, in part because it is a highly dynamic and highly complex region with various physical processes playing an important role, such as the radiative transfer and the thermal conduction along the magnetic field. So far, these properties have not been properly captured in simulations.

Several codes have been developed to model the hydrodynamic response of the atmosphere during solar flares. The first radiative hydrodynamics simulations that considered the thick-target model were performed by Kostiuk & Pikelner (1975); the origin of flare continuum emission in this model was suggested by Livshits *et al.* (1981) and the EUV radiation was modeled by Somov *et al.* (1981). At later times the main effort focused on the evaluating the hydrodynamic response to energy input by injected electrons, assuming a power-law and the thick-target model (Fisher *et al.*, 1985, Canfield & Gayley, 1987, Mariska *et al.*, 1989, Kašparová *et al.*, 2009, Reep *et al.*, 2013, Heinzel *et al.*, 2016). More advanced hydrodynamic codes used to model the effects of electron heating on the atmosphere are, e.g. HYDRAD (Bradshaw & Cargill, 2013), which does not include optically-thick line emission, or FLARIX (Kašparová *et al.*, 2009, Heinzel *et al.*, 2016), which does not solve the linearized equations fully implicitly and computes fewer atoms in detail (e.g. He).

The RADYN code of Carlsson & Stein (1997) has been modified (Abbett & Hawley, 1999, Allred *et al.*, 2015, Rubio da Costa *et al.*, 2015a, Kerr *et al.*, 2016) to simulate the radiative transfer hydrodynamic response of the lower atmosphere to energy deposition

by accelerated electrons in a flare loop. It solves the equations of radiative transfer, atomic level population conservation, and hydrodynamics, covering the sub-photosphere, chromosphere, transition region, and corona. One of the strengths of the code is that it treats the non-LTE radiative transfer in the chromosphere in a fully self-consistent way, providing line intensity, shape, width, Doppler shifts and formation height, and relating them to the heated plasma properties and accelerated particle characteristics. RADYN has been widely used to study the interaction of non-thermal electrons with the lower solar atmosphere (see e.g. Kuridze *et al.*, 2015, Allred *et al.*, 2015, Kennedy *et al.*, 2015, Kowalski *et al.*, 2015, Rubio da Costa *et al.*, 2015b, Kuridze *et al.*, 2016, Kerr *et al.*, 2016, Kowalski *et al.*, 2016, Reid *et al.*, 2017), using an ad-hoc power-law injection model - an approximate procedure to model the energy deposition. Although direct comparison with observed line shapes and intensities is a challenging topic, it has been performed by several authors; i.e. Rubio da Costa *et al.* (2015b), Kennedy *et al.* (2015), and Rubio da Costa *et al.* (2016).

2. Motivation

We aim at a better understanding of the physics in the solar atmosphere by dynamically modeling the energetic connection between the photosphere/chromosphere and corona, giving insights about physical processes that are not yet well understood, such as the coronal heating problem, or how the magnetic energy is released during impulsive events. It is also still unclear how the magnetic energy is transported along the solar atmosphere and converted into heat and particle kinetic energy. The solar community has made some progress in understanding the atmospheric response to eruptive events, but the question where and how the energy is accumulated and stored remains unanswered.

Thanks to the wide range of observations, we are currently able to statistically study eruptive events and get insights from their multi-wavelength emission. For instance, Aschwanden *et al.* (2016) studied the energetics of 191 flares and estimated that the total dissipated magnetic energy E_{mag} exceeds the thermal energy $E_{thermal}$ by 95%. In 71% of the flare events the total dissipated magnetic energy E_{mag} exceeds the non-thermal energy $E_{non_thermal}$, confirming that magnetic reconnection processes are sufficient to explain flare energies. In 85% of the events the non-thermal energy $E_{non_thermal}$ exceeds the thermal energy $E_{thermal}$. Therefore, $E_{mag} > E_{non_thermal} > E_{thermal}$, confirming the thick-target model.

3. Previous theoretical work

Since most of the energy released during solar flares is dissipated in the lower atmosphere (chromosphere/photosphere), we will focus on the results that have been reported so far for this atmospheric layer. The chromospheric layer is a dynamic and radiatively-dominated region that links the optically thick photosphere with the optically thin transition region and corona. Keeping in mind that it is strongly connected with the rest of the atmosphere and its evolution, it is almost impossible to study this atmospheric layer separately; therefore, in order to properly understand the chromosphere, one needs to use a computational domain that covers the atmosphere, from the photosphere to the corona. Also, considering that the chromosphere is dominated by radiation processes, most of the energetically important transitions are far from local thermodynamic equilibrium (LTE).

To address all these difficulties we make use of numerical models, aiming at obtaining physically meaningful results. As already mentioned in § 1, there have been several models developed to model the response of the lower atmosphere to solar flare heating, i.e. the

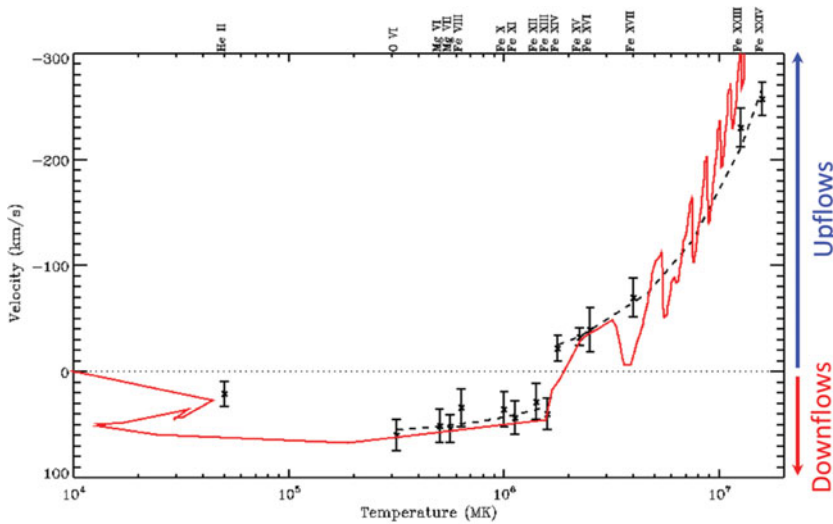


Figure 1. Chromospheric evaporation, resulting from the hydrodynamic response of the atmosphere to flare heating. As a result, there is a temperature break of $T = 17$ MK at which the velocity changes from $v_{downflow} = 60 - 17$ MK to $v_{upflow} = 5 - 17$ MK. © AAS. Reproduced from Liu *et al.* (2009) with permission.

FLARIX code from Varady *et al.* (2014) and references therein. In this manuscript we will focus on the results obtained using the RADYN code (Carlsson & Stein, 1992, Abbett & Hawley, 1999, Allred *et al.*, 2005, 2015), which implicitly solves the following equations: the conservation of mass, momentum, internal energy and charge; the radiative transfer equations; the level population equations; and the atomic abundances for a six-level hydrogen atom, a six-level singly ionized calcium atom, a nine-level helium atom and a four-level singly ionized magnesium atom (see Table 1 in Abbett & Hawley, 1999).

In order to simulate the flare atmosphere from the corona to the photosphere, a non-thermal heating rate term has been introduced in the internal energy equation that considers the flux of energetic, accelerated electrons (Emslie, 1978) and a soft X-ray and EUV irradiation due to the flare heating, such that $\frac{\partial(\rho e)}{\partial t} + \frac{\partial(\rho v e)}{\partial z} + (p + q_v) \frac{\partial v}{\partial z} + \frac{\partial}{\partial z} (F_c + F_r) = Q_{e^-} + Q_{XEUV}$. The heating is injected at the top of a 1-D loop, obtaining the hydrodynamic response of the atmosphere and the emission of the previously mentioned transitions over time.

3.1. Chromospheric evaporation

Milligan *et al.* (2006) have observationally demonstrated that during the impulsive phase of a C9.1 class flare, the evaporated plasma flows upward at several tens of kilometers per second, as a result of non-thermal electrons interacting with the atmosphere. Liu *et al.* (2009) compared these results with their own simulation, combining stochastic acceleration and hydrodynamics, finding a good agreement between both observations and simulations (see Figure 1).

Later, Rubio da Costa *et al.* (2015a) studied how the inclusion of the detailed calculation of the radiative transfer equations, together with stochastic acceleration, affects the atmospheric response by comparing two different models: *PL* for non-thermal electrons following a single power-law, and *SA1* for electrons stochastically accelerated. Figure 2 shows as a results of the simulation that the plasma reaches $30-60 \text{ km s}^{-1}$ downflow

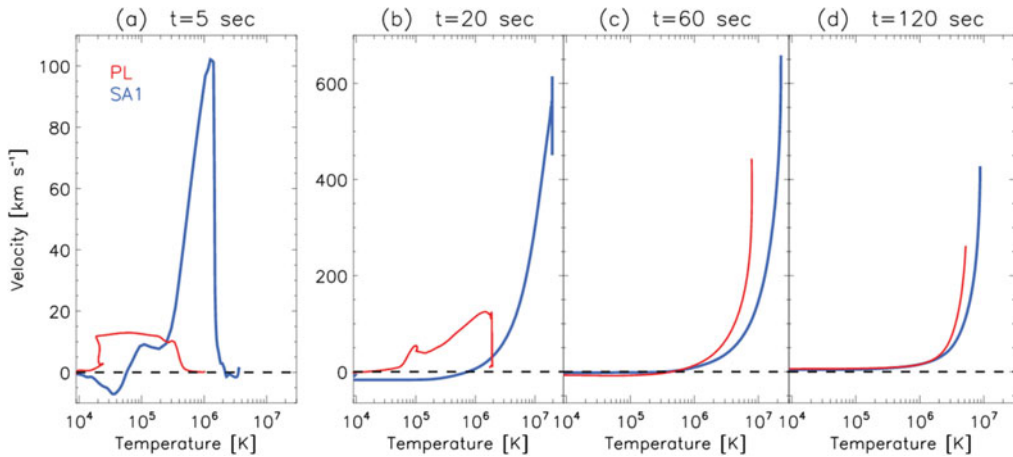


Figure 2. Chromospheric evaporation, from Rubio da Costa *et al.* (2015a). The red line corresponds to a simulation where non-thermal electrons are assumed to follow a single power-law model, and the blue line to electrons considered to have stochastic acceleration.

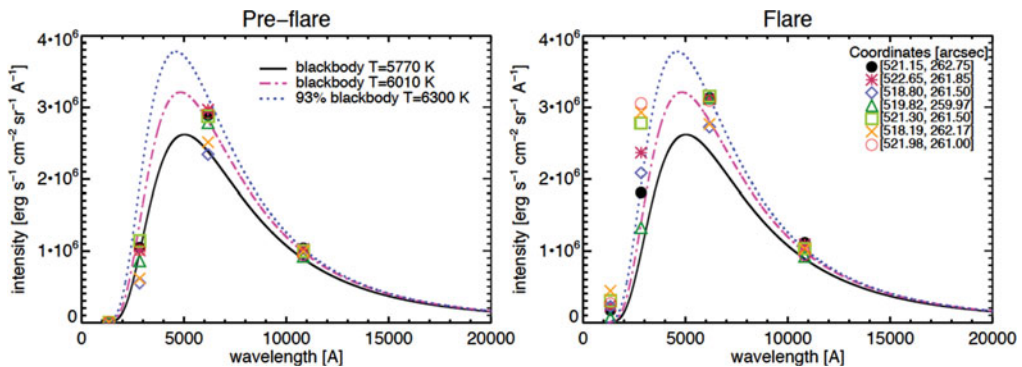


Figure 3. Continuum enhancement during the impulsive phase of an X1.0 class flare (right) with respect the pre-flare emission (left). Figure taken from Kleint *et al.* (2016). © AAS. Reproduced with permission.

speeds within 0.6-1.5 MK at early stages in *SA1*, and a temperature division between up- and downflows of 2 MK, slightly lower than Milligan & Dennis (2009).

3.2. Continuum enhancement

Kleint *et al.* (2016) studied the continuum enhancement during an X1.0 class flare at different wavelengths observationally, and found that the continuum emission in the UV, VIS and IR does not fit to a simple blackbody spectrum, indicating that other processes, such as hydrogen recombination (e.g. Balmer continuum) contribute to the continuum emission (see Figure 3). Using radiative transfer modeling, they found that the hydrogen Balmer continuum emission estimated from 1D static flare models is consistent with the NUV observed emission, but the emission in the optical and IR range is underestimated in the resulting models. They also found that a photospheric temperature increase would increase the optical and IR emission, indicating that both photospheric and chromospheric layers contribute to the continuum radiation during flares.

On the other hand, Kowalski *et al.* (2015) studied the atmospheric response to the injection of non-thermal electrons precipitating towards the lower atmosphere. They estimated the synthetic continuum emission, finding that the photospheric enhancement

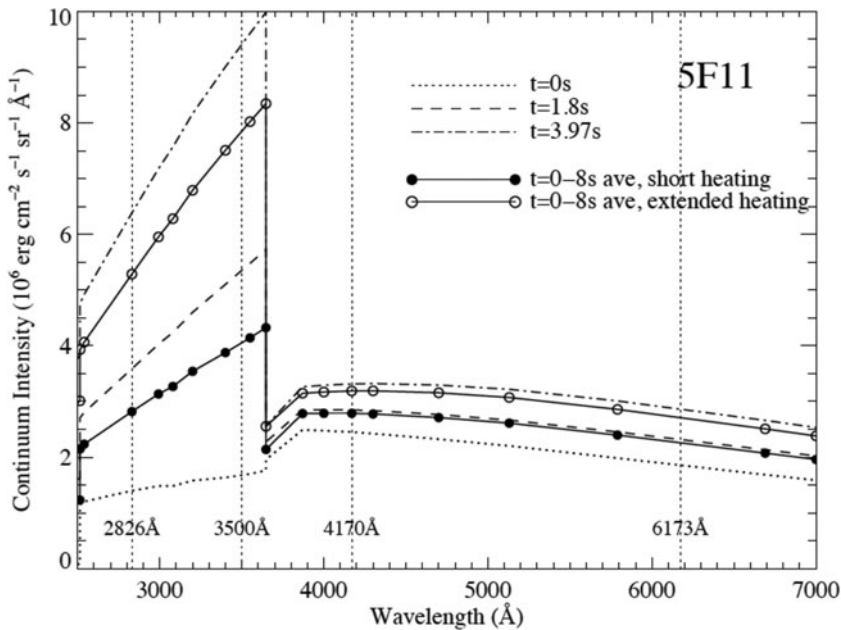


Figure 4. Simulated continuum enhancement, applying a flux of $5 \times 10^{11} \text{ erg s}^{-1} \text{ cm}^{-2}$ (comparable to an X-class flare). Figure from Kowalski *et al.* (2016). © AAS. Reproduced with permission.

during flares can be reproduced with a strong Balmer continuum emission and a smaller contribution from the Paschen recombination, using non-thermal electron fluxes of $10^9 - 10^{11} \text{ erg cm}^{-2} \text{ s}^{-1}$. A higher energy flux of non-thermal electrons ($10^{13} \text{ erg cm}^{-2} \text{ s}^{-1}$) precipitating towards the lower atmosphere is required to reproduce a flare spectrum with a hotter blackbody emission, similar to an M-dwarf, providing an atmosphere that can reproduce the observed bright white-light emission.

Later on, Kowalski *et al.* (2016) used RADYN to simulate the continuum emission and its enhancement, applying a flux of non-thermal electrons of $5 \times 10^{11} \text{ erg s}^{-1} \text{ cm}^{-2}$ (compared to an X-class flare). Although the continuum emission at 2826 Å had increased in their simulations after less than two seconds of heating, it is still at least a factor of two lower than the observed continuum. The continuum enhancement was slightly lower in the far-UV at 1332, 1358, 1389 and 1407 Å (see Figure 4). By comparing the near-UV continuum emission with observations of an X-class flare, they found that the hydrogen Balmer recombination radiation originating at low optical depth in the chromosphere can reproduce the observed continuum emission.

3.3. Line profiles

The community has shown an effort in understanding the chromospheric emission during solar flares, focusing on studying the evolution of several chromospheric line profiles. For instance, Kuridze *et al.* (2015) studied the temporal evolution of the synthetic H α and CaII 8542 Å profiles using the modified code of Allred *et al.* (2015) with a flux beam of $10^{11} \text{ erg cm}^{-2} \text{ s}^{-1}$, concluding that the red asymmetries shown in the H α profiles may not be related with plasma downflows.

Kennedy *et al.* (2015) aimed at studying an X1.5 class flare and estimated the electron heating rate from *RHESSI* observations. They compared the synthetic HeII 304 Å light

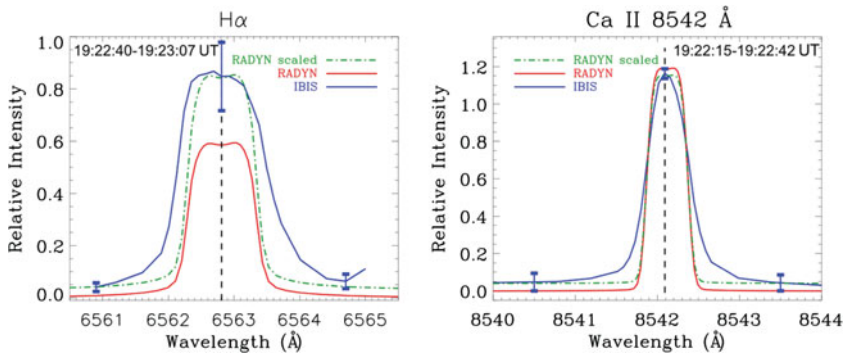


Figure 5. Temporal evolution of the synthetic $H\alpha$ and $CaII$ 8542 Å profiles, from Rubio da Costa *et al.* (2015b).

curve emission with observations from EVE *MEGS-A*, finding a good agreement between them.

Kerr *et al.* (2016) have studied the $MgII$ k and $CaII$ 8542 Å emission as a result of the atmospheric heating via damping of Alfvén Waves traveling downward through the chromosphere, following the estimation of the heating rate described by Reep & Russell (2016). They found that Alfvén wave dissipation is effective in heating the chromosphere. Comparing their line profiles with the ones resulting from non-thermal electrons having an ad-hoc single power-law, they found that the $CaII$ 8542 Å profiles are similar, while the $MgII$ spectra present at certain times a single peaked, redshifted line core with an extended blue wing.

Kuridze *et al.* (2016) studied the evolution of the NaI D_1 line profiles of an M3.9 class flare using IBIS observations. They estimated the electron heating rate from *RHESSI* observations and run the RADYN code of Allred *et al.* (2015) to estimate the atmospheric response to the flare heating. Using the RH radiative transfer code of Uitenbroek (2001), they obtained the synthetic NaI D_1 line profiles. They found that the line profile turns into emission with the initiation of the beam heating (without a central reversal) and as soon as the beam heating is turned off, the profile shows a centrally reversed core with asymmetries in the line wings.

There have been several attempts to compare the synthetic line profiles with observations. For the first time, Rubio da Costa *et al.* (2015b) and Rubio da Costa *et al.* (2016) compared synthetic $H\alpha$ and $CaII$ 8542 Å line profiles with observations from an M3.0 and X1.0 class flare, respectively. Figure 5 compares the synthetic $H\alpha$ and $CaII$ 8542 Å line profiles with DST/IBIS observations.

Kowalski *et al.* (2016) used an electron beam of 5×10^{11} erg cm^{-2} s^{-1} in the RADYN code and studied not only the continuum emission as discussed in § 3.2, but also the $FeII$ 2814.45 Å line profiles. In Figure 6, they compared the $FeII$ 2814.45 Å line profile with observations, finding that the synthetic $FeII$ 2814.45 Å emission is overestimated by a factor of 2.

Rubio da Costa *et al.* (2016) studied the same X1.0 flare as Kowalski *et al.* (2016), but focused on the chromospheric emission in $H\alpha$ and $CaII$ 8542 Å resulting from RADYN and the $MgII$ emission resulting from the RH code. While the synthetic $H\alpha$ and $CaII$ 8542 Å profiles reproduce the observations, the *IRIS* $MgII$ duplet presents broader line profiles than the synthetic ones. As Leenaarts *et al.* (2013) discuss, this difference could be affected by the 3D effects in radiative transfer calculations, not included in the RADYN/RH simulations. They explored the constraints that $MgII$ profiles set on the

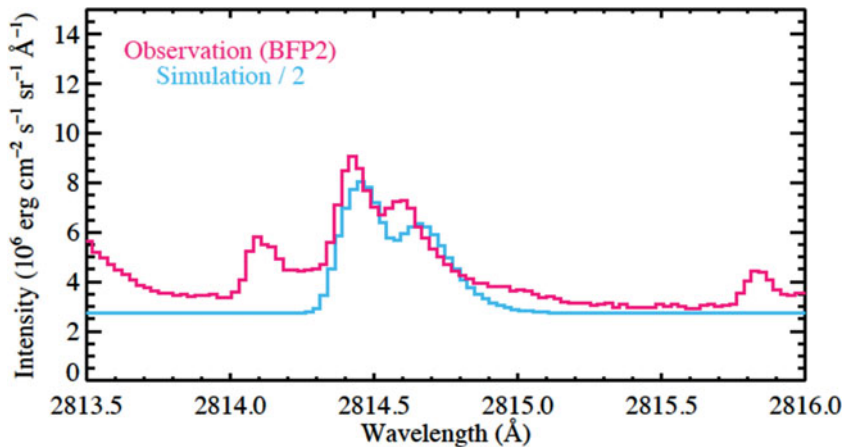


Figure 6. Comparison of the FeII 2814Å synthetic line emission with *IRIS* observations from an X1.0 class flare. Figures taken from Kowalski *et al.* (2016). © AAS. Reproduced with permission.

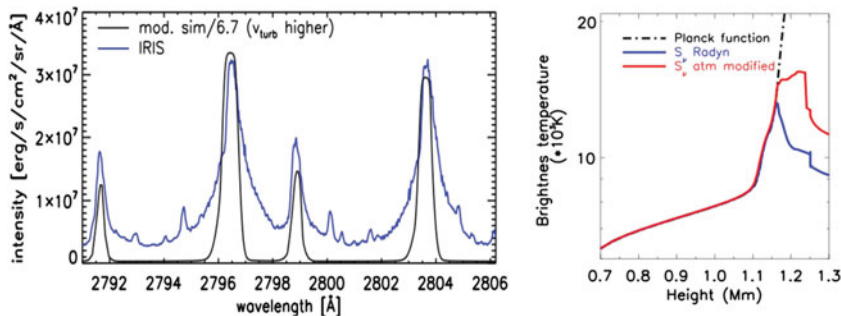


Figure 7. [Left]: Comparison of the MgII h&k line profiles from a modified atmosphere with *IRIS* observations (Rubio da Costa *et al.*, 2016); [Right]: Planck function (black) and source function S_ν resulting from the original atmosphere (blue), and after increasing the electron density in the upper chromosphere (red).

chromospheric structure, and found that the temperature increase or density increase in the upper chromosphere results in a single peak core (see Figure 7 [left]). The line core is formed in this simulation in a narrow region of ~ 800 km, at a height of 1.23 Mm; by increasing the temperature or density, one couples the source function to the Planck function (see Figure 7 [right]). To fit the narrow line core and the very broad line wings, they also included a microturbulent velocity of 27 km s^{-1} in the narrow region where the wings are formed.

4. Discussion and further steps

Kowalski *et al.* (2015) and Kowalski *et al.* (2016) have studied the contribution of an electron beam heating to the continuum emission, finding that the white-light emission shows a significant increase during solar flares, as seen in observations (i.e. Kleint *et al.*, 2016).

Several authors have qualitatively compared the simulated line emissions with *IRIS* and DST/IBIS observation at various wavelengths, but there have been few attempts to directly compare line profiles (Rubio da Costa *et al.*, 2015b, Rubio da Costa *et al.*, 2016) or integrated light curves (i.e. Kuridze *et al.*, 2016). So far all studies agree that

the synthetic line profiles are too narrow and the broad wings are not yet reproduced by the simulations.

Kennedy *et al.* (2015), Rubio da Costa *et al.* (2015b), Rubio da Costa *et al.*, 2016 and Kuridze *et al.* (2016) have used *RHESSI* spectra to estimate the variation of the non-thermal component of the electron spectra parameters, assuming an ad-hoc single power-law. This can be improved by fitting the spectra with a forward fitting procedure (Chen & Petrosian, 2013).

As a step forward, we aim at using the combined Stanford Fokker-Planck acceleration-transport code (Petrosian & Liu, 2004) and RADYN, following the method of Rubio da Costa *et al.* (2015a), achieving a more accurate determination of the radiative signatures of the flare.

As Kowalski *et al.* (2015) previously mentioned, the results obtained using the RADYN code can be improved by including the cooling from MgII and FeII ions, and non-thermal ionization of HI and HeII in the model.

The main goal is to get feedback from flaring observations at different wavelength ranges covering the whole atmosphere, to be able to compare them with the synthetic emission, to understand how the atmosphere responds to a flare heating at different heights, and to get insights about the energy deposition.

Acknowledgements

Work performed by F.R.dC. is supported by NASA grants NNX13AF79G and NNX14AG03G. F.R.dC. thanks ISSI and ISSI-BJ for the support of the team “Diagnosing heating mechanisms in solar flares through spectroscopic observations of flare ribbons”. We gratefully acknowledge the use of supercomputer resources provided by the NASA High-End Computing (HEC) Program through the NASA Advanced Supercomputing (NAS) Division at Ames Research Center. The author thanks K. Schindler for proofreading and the helpful discussions. This research has made use of NASA’s Astrophysics Data System.

References

- Abbett, W. P. & Hawley, S. L. 1999, *ApJ*, 521, 906
 Allred, J. C., Hawley, S. L., Abbett, W. P., & Carlsson, M. 2005, *ApJ*, 630, 573
 Allred, J. C., Kowalski, A. F., & Carlsson, M. 2015, *ApJ*, 809, 104
 Aschwanden, M. J., Holman, G., O’Flannagain, A., *et al.* 2016, *ApJ*, 832, 27
 Bradshaw, S. J. & Cargill, P. J. 2013, *ApJ*, 770, 12
 Canfield, R. C. & Gayley, K. G. 1987, *ApJ*, 322, 999
 Carlsson, M. & Stein, R. F. 1992, *ApJ* (Letters), 397, L59
 Carlsson, M. & Stein, R. F. 1997, *ApJ*, 481, 500
 Chen, Q. & Petrosian, V. 2013, *ApJ*, 777, 33
 Emslie, A. G. 1978, *ApJ*, 224, 241
 Fisher, G. H., Canfield, R. C., & McClymont, A. N. 1985, *ApJ*, 289, 414
 Heinzel, P., Kasparova, J., Varady, M., Karlický, M., & Moravec, Z. 2016, arXiv:1602.00016
 Kašparová, J., Varady, M., Heinzel, P., Karlický, M., & Moravec, Z. 2009, *A&A*, 499, 923
 Kennedy, M. B., Milligan, R. O., Allred, J. C., Mathioudakis, M., & Keenan, F. P. 2015, *A&A*, 578, A72
 Kerr, G. S., Fletcher, L., Russell, A. J. B., & Allred, J. C. 2016, *ApJ*, 827, 101
 Kleint, L., Heinzel, P., Judge, P., & Krucker, S. 2016, *ApJ*, 816, 88
 Kostiuik, N. D. & Pikelner, S. B. 1975, *Sov. Astr.*, 18, 590
 Kowalski, A. F., Hawley, S. L., Carlsson, M., *et al.* 2015, *Sol. Phys.*, 290, 3487
 Kowalski, A. F., Allred, J. C., Daw, A. N., Cauzzi, G., & Carlsson, M. 2016, arXiv:1609.07390

- Kuridze, D., Mathioudakis, M., Simões, P. J. A., *et al.* 2015, *ApJ*, 813, 125
- Kuridze, D., Mathioudakis, M., Christian, D. J., *et al.* 2016, *ApJ*, 832, 147
- Leenaarts, J., Pereira, T. M. D., Carlsson, M., Uitenbroek, H., & De Pontieu, B. 2013, *ApJ*, 772, 90
- Liu, W., Petrosian, V., & Mariska, J. T. 2009, *ApJ*, 702, 1553
- Livshits, M. A., Badalian, O. G., Kosovichev, A. G., & Katsova, M. M. 1981, *Sol. Phys.*, 73, 269
- Mariska, J. T., Emslie, A. G., & Li, P. 1989, *ApJ*, 341, 1067
- Milligan, R. O., Gallagher, P. T., Mathioudakis, M., & Keenan, F. P. 2006, *ApJL*, 642, L169
- Milligan, R. O. & Dennis, B. R. 2009, *ApJ*, 699, 968
- Petrosian, V. & Liu, S. 2004, *ApJ*, 610, 550
- Reid, A., Mathioudakis, M., Kowalski, A., Doyle, J. G., & Allred, J. C. 2017, arXiv:1701.04213
- Reep, J. W., Bradshaw, S. J., & McAteer, R. T. J. 2013, *ApJ*, 778, 76
- Reep, J. W. & Russell, A. J. B. 2016, *ApJL*, 818, L20
- Rubio da Costa, F., Liu, W., Petrosian, V., & Carlsson, M. 2015, *ApJ*, 813, 133
- Rubio da Costa, F., Kleint, L., Petrosian, V., Sainz Dalda, A., & Liu, W. 2015, *ApJ*, 804, 56
- Rubio da Costa, F., Kleint, L., Petrosian, V., Liu, W., & Allred, J. C. 2016, *ApJ*, 827, 38
- Somov, B. V., Spektor, A. R., & Syrovatskii, S. I. 1981, *Sol. Phys.*, 73, 145
- Uitenbroek, H. 2001, *ApJ*, 557, 389
- Varady, M., Karlický, M., Moravec, Z., & Kašparová, J. 2014, *A&A*, 563, A51